DINAME 2019 - Proceedings of the XV International Symposium on Dynamic Problems of Mechanics,
M.A. Savi, T.G. Ritto and W.M. Bessa (Editors), ABCM, Buzios, RJ, Brazil, March 10th to 15th, 2019

Nonlinear vibrations analysis of a conoidal shell

Cássio L. R. Moreira [1], Renata M. Soares [1], Frederico Martins Alves da Silva [1]

[1] School of Civil and Environmental Engineering- Federal University of Goiás. Av. Universitária, nº 1488-St. Universitário. CEP 74605-200, Goiania-Brazil.

Abstract: Conoidal shells are lightweight structures that are often used as roofing in civil construction due to their pleasant and modern aesthetics, as well as allowing the entry of natural light, presenting ease of execution and good structural performance. To fully understand the behavior of these structures it is necessary to analyze them considering the geometric nonlinearity of the problem. In this work, a static and dynamic nonlinear analysis of a conoidal shell made of homogeneous, isotropic and linear elastic material, submitted to a uniformly distributed load in the transverse direction, is made with the aid of the commercial finite element software ABAQUS®. The natural frequency of this shell and its corresponding vibration mode is obtained as well as the nonlinear equilibrium path, the frequency-load relation, the frequency-amplitude relation and the phase portrait diagram for forced vibration. Results show the softening behavior of these structures and the occurrence of snap through for certain dynamic perturbations.

Keywords: Conoidal shell, Nonlinear vibration, Natural frequency, Finite element method.

INTRODUCTION

Conoidal shells are ruled surfaces that are obtained by the translations of a master plane along a straight-line intersecting with other straight or curved lines that gives its geometry. They are often used as roofing for its constructive advantages when compared to other shells that have curvature in both directions since the geometry of the conoidal shell can be obtained by the overlap of several straight lines segments as beams or bars. This implies less cost with casting and ease of execution. In addition, they also allow the entrance of natural light and present a modern and pleasant aesthetic.

It is shown by Debongnie (1978) that it is possible to obtain the equilibrium equations of the conoidal shell using the Marguerre's shallow shell theory, in which a fictious displacement that represents the geometry of the conoid is inserted on a plate as a geometric imperfection. Since the equilibrium equations has no closed form solution, these problems are often solved by a semi analytic approach, as the Galerkin method, or a purely numerical approach as the finite element method.

In this sense, the static bending of conoidal shell was analyzed by Bandyopadhyay e Ghosh (1989) using a finite element formulation and later by Bandyopadhyay e Ghosh (1990) using the Galerkin method. Badyopadhyay, Chakravorty e Sinha (1995), also numerically, shows the effect of the conoidal geometry on its natural frequency. Similarly, the effect on the stiffness of these structures is verified by Badyopadhyay e Nayak (2002) due to the presence of stiffening beams and by Chakravorty e Hota (2007) due to cutouts in its geometry. Recently, Cavalcanti (2014) explores the effect of different geometry and boundary conditions on the buckling and free vibration response of the conoidal shell and Morais (2017) verifies its post buckling nonlinear behavior. In the other hand, Gonçalves e Soares (2015) and Gonçalves e Soares (2016) obtained the nonlinear time response for free and forced damped vibration.

The aim of this work is to verify, using the commercial software of finite elements ABAQUS®, the static and dynamic nonlinear behavior of a parabolic conoidal shell composed of homogeneous linear elastic isotropic material submitted to a uniformly distributed transverse load. Therefore, the nonlinear equilibrium path, load-frequency of vibration relation, frequency-amplitude relation and the phase portrait diagrams are analyzed in order to better understand this structure's behavior.

MATHEMATICAL FORMULATION

Considering a conoidal shell of length a, width $2b$, higher arch height H_h, lower arch height H_l, thickness h, made of homogeneous linear elastic isotropic material with Young's modulus E, Poisson coefficient v and density ρ, as shown in Fig. 1.

According to Bandyopadhyay e Ghosh (1989a), the surface of the parabolic conoid is obtained by the Eq. (1).

$$w_0 = -H_h\left[1-\left(1-\frac{H_l}{H_h}\right)\frac{x}{a}\right]\left[1-\frac{y^2}{b^2}\right] \tag{1}$$

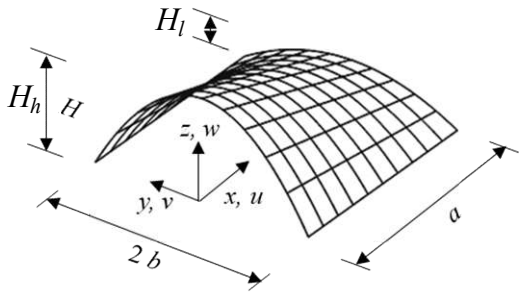

Figure 1 – Parabolic conoidal shell geometry

The transverse loading uniformly distributed per unit of horizontal area is obtained by the Eq. (2) in which p is the magnitude of the gravitational load per unit of surface area.

$$p_z = p\left[1+\frac{\partial w_0}{\partial x}^2+\frac{\partial w_0}{\partial y}^2\right]^{1/2} \tag{2}$$

Assuming Kirchhoff hypothesis, the displacement field for an arbitrary point of the shell can be written as shown in Eqs. (3)-(5) in which u, v and w are the displacements in x, y and z directions respectively and the geometry of the parabolic conoid is inserted as a geometric imperfection given by w_0 in Eq. (5).

$$\overline{u} = u(x,y) - z\,w(x,y)_{,x} \tag{3}$$

$$\overline{v} = v(x,y) - z\,w(x,y)_{,y} \tag{4}$$

$$\overline{w} = w(x,y) + w_0(x,y) \tag{5}$$

Considering the strains to be small, the strain-displacement relations for an arbitrary point is given by Eqs. (6)-(8).

$$\overline{\varepsilon}_x = \varepsilon_x - z\,\overline{w}_{,xx} \tag{6}$$

$$\overline{\varepsilon}_y = \varepsilon_y - z\,\overline{w}_{,yy} \tag{7}$$

$$\overline{\gamma}_{xy} = \gamma_{xy} - 2\,z\,\overline{w}_{,xy} \tag{8}$$

And based on von Karman plate theory, starting with no initial stress or strain, the strain-displacement for a point in the middle surface is given by Eqs. (9)-(11).

$$\varepsilon_x = u_{,x} + \frac{1}{2}w_{,x}^2 + w_{,x}w_{0,x} \tag{9}$$

$$\varepsilon_y = v_{,y} + \frac{1}{2}w_{,y}^2 + w_{,y}w_{0,y} \tag{10}$$

$$\gamma_{xy} = u_{,y} + v_{,x} + w_{,x}w_{,y} + w_{,x}w_{0,y} + w_{,y}w_{0,x} \tag{11}$$

Considering a shell made of homogeneous linear elastic isotropic material the stress components are given by Eq. (12).

$$\begin{Bmatrix}\overline{\sigma}_x\\ \overline{\sigma}_y\\ \overline{\tau}_{xy}\end{Bmatrix} = \frac{E}{\left(1-\nu^2\right)}\begin{bmatrix}1 & \nu & 0\\ \nu & 1 & 0\\ 0 & 0 & \frac{1-\nu}{2}\end{bmatrix}\begin{Bmatrix}\overline{\varepsilon}_x\\ \overline{\varepsilon}_y\\ \overline{\gamma}_{xy}\end{Bmatrix} \tag{12}$$

The normal and moments resultants per length unit are obtained by the integration of the stress components along the thickness as shown in Eqs (13)-(14).

$$n_x = \int_{-h/2}^{h/2} \overline{\sigma}_x \, dz \qquad n_y = \int_{-h/2}^{h/2} \overline{\sigma}_y \, dz \qquad n_{xy} = n_{yx} = \int_{-h/2}^{h/2} \overline{\tau}_{xy} \, dz \tag{13}$$

$$m_x = \int_{-h/2}^{h/2} \overline{\sigma}_x \, z \, dz \qquad m_y = \int_{-h/2}^{h/2} \overline{\sigma}_y \, z \, dz \qquad m_{xy} = m_{yx} = \int_{-h/2}^{h/2} \overline{\tau}_{xy} \, z \, dz \tag{14}$$

In this sense, the equations of motion are obtained, adding the inertial and damping forces, either by summation of forces in a deformed infinitesimal element of shell, or by variational methods using the stationary energy principle, and they are written in terms of the displacements of the middle surface and the imperfection function as shown in Eqs (15)-(17). In which $D = Eh^3/[12(1-\nu^2)]$ and $C = Eh/(1-\nu^2)$ are, respectively, the flexural and membrane shell stiffness parameters.

$$\begin{aligned} &u_{,xx} + w_{,x}\, w_{,xx} + w_{,x}\, w_{0,xx} + w_{,xx}\, w_{0,x} + \nu\left(v_{,xy} + w_{,y}\, w_{,xy} + w_{,y}\, w_{0,xy} + w_{,xy}\, w_{0,y}\right) \\ &+ \frac{1-\nu}{2}\left(u_{,yy} + v_{,xy} + w_{,xy}\, w_{,y} + w_{,x}\, w_{,yy} + w_{,xy}\, w_{0,y} + w_{,x}\, w_{0,yy} + w_{0,xy}\, w_{,y} + w_{0,x}\, w_{,yy}\right) = 0 \end{aligned} \tag{15}$$

$$\begin{aligned} &v_{,yy} + w_{,y}\, w_{,yy} + w_{,y}\, w_{0,yy} + w_{,yy}\, w_{0,y} + \nu\left(u_{,xy} + w_{,x}\, w_{,xy} + w_{,x}\, w_{0,xy} + w_{,xy}\, w_{0,x}\right) \\ &+ \frac{1-\nu}{2}\left(v_{,xx} + u_{,xy} + w_{,xy}\, w_{,x} + w_{,y}\, w_{,xx} + w_{,xy}\, w_{0,x} + w_{,y}\, w_{0,xx} + w_{0,xy}\, w_{,x} + w_{0,y}\, w_{,xx}\right) = 0 \end{aligned} \tag{16}$$

$$\begin{aligned} &D\nabla^4 w - C\Big\{u_{,x}\left(w+w_0\right)_{,xx} + \nu\, v_{,y}\left(w+w_0\right)_{,xx} + \frac{1}{2} w_{,x}{}^2\left(w+w_0\right)_{,xx} + \frac{\nu}{2} w_{,y}{}^2\left(w+w_0\right)_{,xx} \\ &+ w_{,x}\, w_{0,x}\left(w+w_0\right)_{,xx} + \nu\, w_{,y}\, w_{0,y}\left(w+w_0\right)_{,xx} + (1-\nu)\Big[u_{,y}\left(w+w_0\right)_{,xy} + v_{,x}\, w_{,xy} \\ &+ w_{,x}\, w_{,y}\left(w+w_0\right)_{,xy} + w_{,x}\, w_{0,y}\left(w+w_0\right)_{,xy} + w_{,y}\, w_{0,x}\left(w+w_0\right)_{,xy}\Big] \\ &+ u_{,y}\, w_{,yy} + \nu\, v_{,x}\, w_{,yy} + \frac{1}{2} w_{,y}{}^2\, w_{,yy} + \frac{\nu}{2} w_{,x}{}^2\, w_{,yy} + w_{,y}\, w_{0,y}\, w_{,yy} + \nu\, w_{,x}\, w_{0,x}\, w_{,yy}\Big\} \\ &= p_z - \rho\, h\, \ddot{w} - c\, h\, \dot{w} \end{aligned} \tag{17}$$

It is seen that this system has nonlinear partial differential equations with quadratic and cubic terms, with coupled displacements and highly dependent on the imperfection function. As shown by Bandyopadhyay e Ghosh (1989), in order to solve this system of equations, an appropriate function that describes the displacements, boundary condition and internal stresses of this structure is needed. Morais (2017) uses a Fourier series expansion to the displacements u, v and w but the results didn't achieve a desired precision due to the number of terms necessary to describe the conoidal's displacements. Since it has no closed form solution, an approximate numeric solution is obtained using the finite element method. In this sense, the terms that appears in this system of equations of motion and their degree can be used to better understanding the numerical results given by a purely numerical method.

NUMERICAL RESULTS

Considering a conoidal shell of length $a = 6$ m, width $2b = 8$ m, three different higher arch height $H_h = 0.1$ m; $H_h = 1.0$ m and $H_h = 1.5$ m, lower arch height $H_l = 0$, thickness $h = 0.06$ m, made of homogeneous linear elastic isotropic material with Young's modulus $E = 14$ GPa, Poisson coefficient $\nu = 0.3$ and density $\rho = 2500\text{kg/m}^3$. The straight boundaries are supported while the curved boundary is free. The finite element software ABAQUS® is used to obtain the linear and nonlinear results. A mesh convergence study is made showing that accurate results are obtained with 768 S4R shell elements.

Linear Results

Initially, the first natural vibration mode and its associated frequency, for each case of geometry, are obtained solving a linear eigenvalue problem as shown in Figs. 2-4. The first vibration mode has a natural frequency of vibration

$\omega_1 = 21.5$ rad/s for $H_h = 0.10$ m, $\omega_1 = 72.0$ rad/s for $H_h = 1.00$ m and $\omega_1 = 86.7$ rad/s for $H_h = 1.50$ m. They are flexional modes, and they have the predominant displacements occurring in the transverse (z) direction, as illustrated in Figs. 2(c), 3(c) and 4(c). However, it is observed that the vibration mode changes as H_h increases, also the magnitude of displacements in the x and y directions becomes significant with the increase of the higher arc's height when they are compared with transversal displacements. This can be justified by the presence of w_0 in Eqs. (15) and (16).

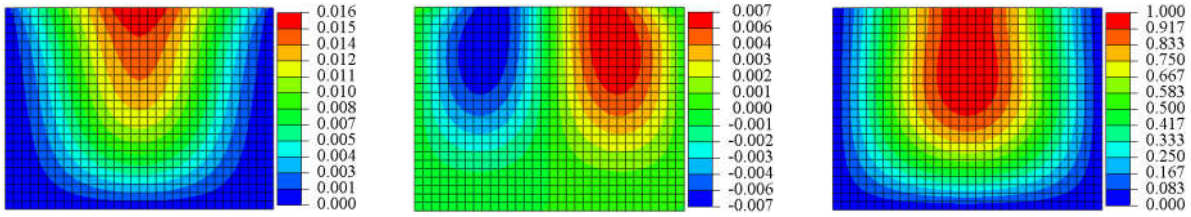

(a) Displacement u (b) Displacement v (c) Displacement w

Figure 2 – First vibration mode for $H_h = 0.10$ m; $\omega_1 = 21.5$ rad/s

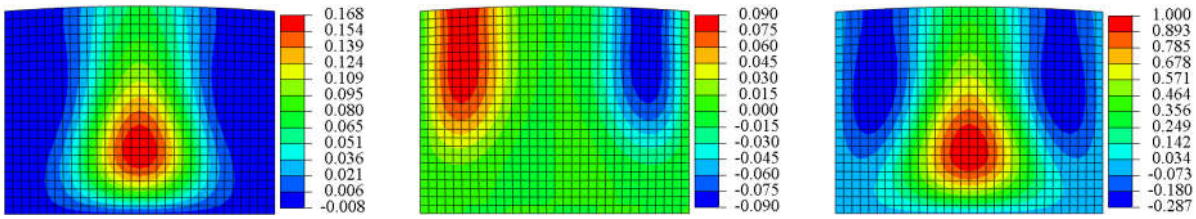

(a) Displacement u (b) Displacement v (c) Displacement w

Figure 3 – First vibration mode for $H_h = 1.00$ m; $\omega_1 = 72.0$ rad/s

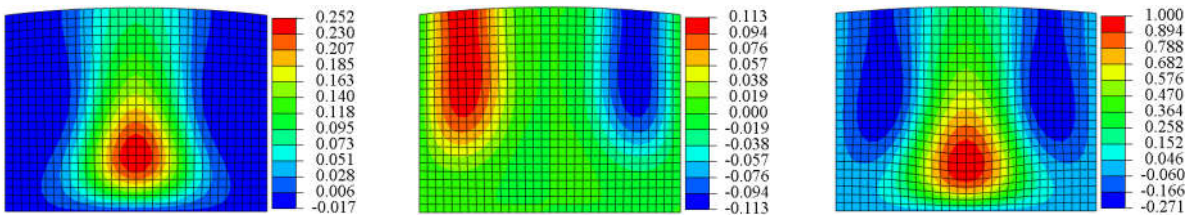

(a) Displacement u (b) Displacement v (c) Displacement w

Figure 4 – First vibration mode for $H_h = 1.50$ m; $\omega_1 = 86.7$ rad/s

Nonlinear results

The nonlinear equilibrium path, when a uniform transversal distributed load p is applied, is determined using the Riks method. In this method, both forces and displacements are variables to be solved and it is recommended in problems that show unstable geometrically nonlinear collapse. The curves distributed load versus transverse displacement are shown in Fig. 5. The displacements are taken in the transverse (z) direction at the points that show maximum value of displacement in the first vibration mode presented i.e. (x, y) = (0.0, 0.0) for $H_h = 0.10$ m; (x, y) = (4.0, 0.0) for $H_h = 1.00$ m and (x, y) = (4.5, 0.0) for $H_h = 1.50$ m.

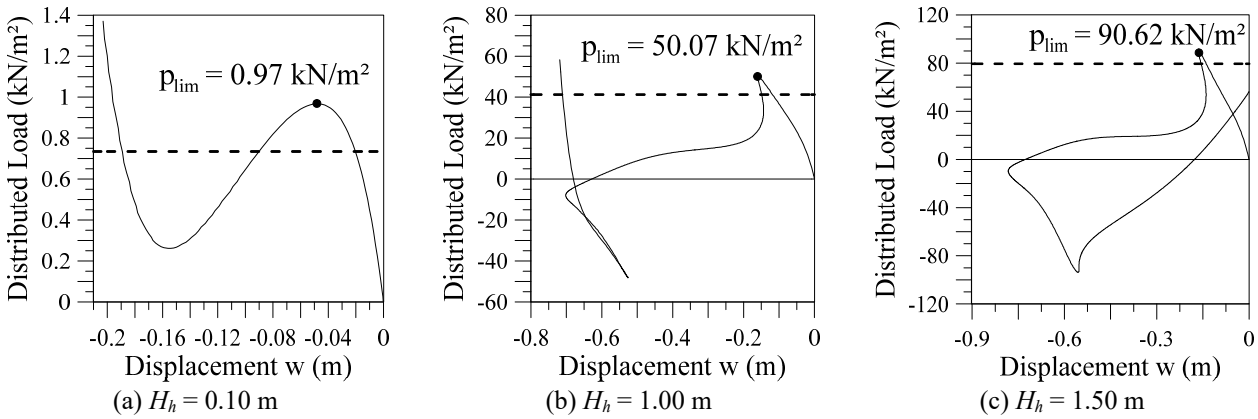

(a) $H_h = 0.10$ m (b) $H_h = 1.00$ m (c) $H_h = 1.50$ m

Figure 5 – Static nonlinear equilibrium path

The dot in Fig. 5 represents the limit load achieved and, as expected, higher values of H_h increases the load limit and changes the nonlinear equilibrium path. For $H_h = 0.10$ m, Fig. 5(a), a classical snap through response is obtained. For $H_h = 1.00$ m, Fig. 5(b), and $H_h = 1.50$ m, Fig. 5(c), both snap through and snap back phenomena occur and also the inversion of the load capacity of the structure due to the nonlinear w_0 terms that appear in the Eqs. (15)-(17).

Let p_{lim} (represented by the dot in Fig. 5) be the first maximum value of load achieved in order to verify the variation of the natural frequency of vibration with the increase of the load up to p_{lim}. As shown in Fig. 6, the natural frequency of vibration decreases as the magnitude of the load p increases up to the load p_{lim} when the natural frequency of vibration becomes null meaning the structure becomes unstable due to the compressive stresses that occur in the structure. Also, this nonlinear relation changes as H_h increases with no clear proportionality.

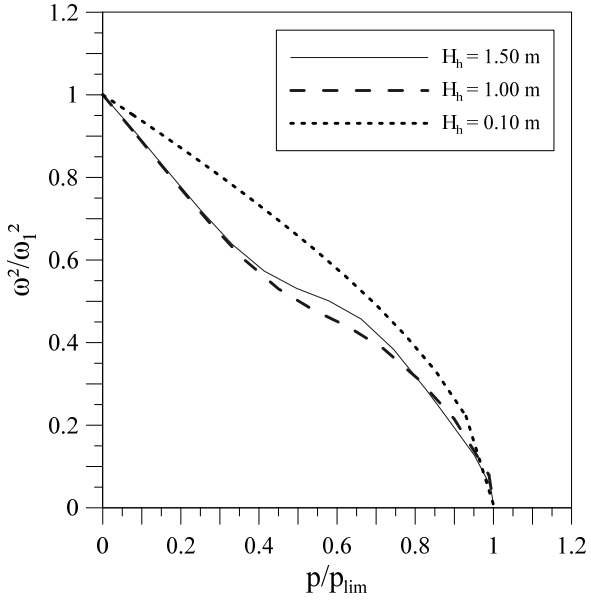

Figure 6 – Load *versus* frequency of vibration

The nonlinear frequency-amplitude relation associated with the first mode of vibration is obtained numerically for $H_h = 0.10$ m and $H_h = 1.00$ m using a similar methodology to the one proposed by Nandakumar and Chatterjee (2005). An initial condition of displacement equal to the first mode of vibration (Figs. 2-3) is applied to the structure and then the time response in a chosen point (same point used to plot Fig. 5) for the free vibration is obtained using a slightly damped system. The Rayleigh viscous damping model is used, in which the damping coefficient $\xi_i = \alpha/(2\omega_i) + \beta\omega_i/2$, where α and β are the Rayleigh coefficients proportional to the mass and stiffness respectively. In the subsequent analysis is used $\alpha = 0$ and β is indicated in each case since it must be chose accordingly to the structure's frequency of vibration.

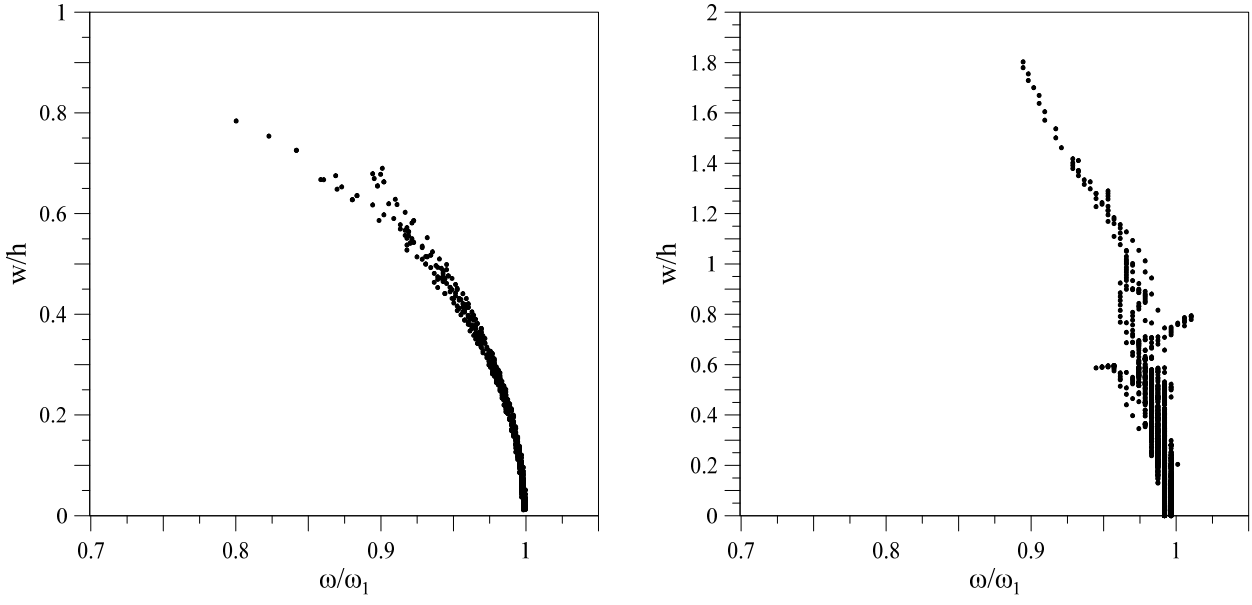

(a) $H_h = 0.10$ m; $\beta = 9e\text{-}4$ (b) $H_h = 1.00$ m; $\beta = 2.5e\text{-}4$

Figure 7 – Nonlinear frequency-amplitude relation

At each wave (three nodes and two antinodes, one positive and the other negative), the frequency of vibration is obtained by the inverse of the wavelength, and the amplitude of vibration is obtained by the mean of the absolute value of the antinodes amplitudes. Figure 7 shows the frequency-amplitude relation normalized with the thickness of the shell and its natural linear frequency of vibration. The scatter of points is due to the time step used in the integration of the 4950 equations of motion of this problem i.e. a smother curve could be obtained using a smaller time step and more computational effort.

It is observed a softening behavior in nonlinear frequency-amplitude relation (backbone curve), the decrease of the stiffness of the structure with increasing of the displacements. For $H_h = 0.10$ m, up to 20% of the stiffness decreases when the displacements are large (near the thickness magnitude) and $H_h = 1.00$ m this decrease is 10% when the displacement is nearly twice the thickness.

For the forced damped vibration response, a distributed load p_i (represented by the dashed line in Fig. 5) is applied as a static load and a ratio of this value, k, is applied as a harmonic load as shown in the Eq. (18), in which Ω is the load excitation frequency assumed to be equal to the first natural frequency of vibration and t is the time in seconds. To obtain the Poincare section using a finite element procedure, the time step used in the integration of the equations of motion is a ratio of the period of the structure, hence it is possible to collect in the time response the displacement and velocity at each Poincare section with the aid of a simple procedure.

$$p(t) = p_i\left[1 + k\sin\left(\Omega t\right)\right] \tag{18}$$

For $H_h = 0.10$ m and $p_i = 0.735$ kN/m² there is three equilibrium positions (Fig. 5a). For a small dynamic perturbation, the structure oscillates around the lowest equilibrium position (w = -0.02 m) as can be seen in the Fig. 8a. However, for a higher perturbation a dynamic jump occurs (snap through phenomenon) and the structure oscillates around the highest equilibrium position (w = -0.18 m) instead (Fig. 8b) indicating that this equilibrium position is a stable one. In other words, after the structure loses its stability (Fig. 6a), it can become stable again. Figure 8c shows the phase portrait diagram for these two orbits and also theirs Poincare section in which can be verified to be a periodicity one response.

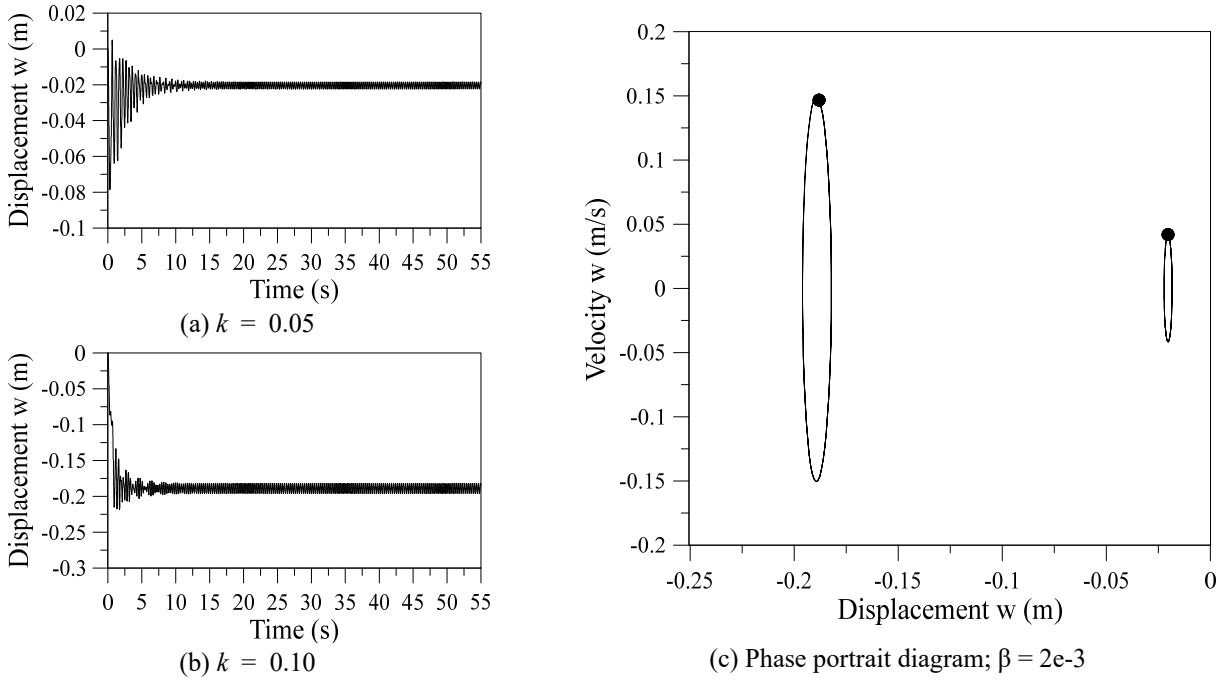

(a) k = 0.05

(b) k = 0.10

(c) Phase portrait diagram; β = 2e-3

Figure 8 – H_h = 0.10 m; p_i = 0.735 kN/m²

For $H_h = 1.00$ and $p_i = 41.22$ kN/m² there are three equilibrium positions in Fig. 6b. Counterintuitively, for $k = 0.05$ the snap through occurs and the structure vibrates around w = -0.71 m (Fig. 9a) while for a higher dynamic perturbation ($k = 0.10$) the structure stabilizes at the lower equilibrium position w = -0.11 m (Fig. 9b) and the snap through does not occur in the time period analyzed. Figure 9c shows the phase portrait diagram and the Poincare section of these responses showing them to have a periodicity one. This response can be explained by the existence of a complex bifurcation diagram, assuming k as a control parameter.

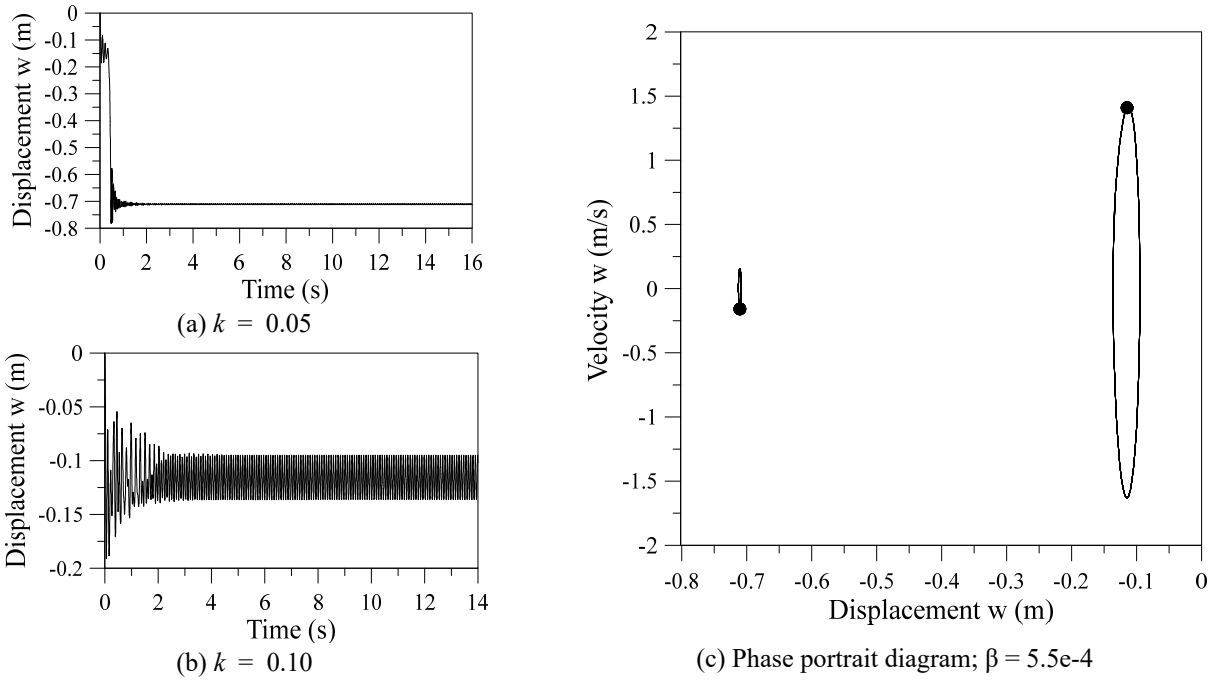

Figure 9 – H_h = 1.00 m; p_i = 41.22 kN/m²

For H_h = 1.50 and p_i = 79.5 kN/m², Fig. 6c shows two equilibrium positions. For k = 0.05 the structure oscillates around w = -0.14 m (Fig. 10a), this position can be seen in the equilibrium path (Fig 6c). However, for k = 0.10 the structure oscillates around w = -0.8 m (Fig. 10b), this indicate that there is a stable equilibrium configuration at this displacement. Figure 10c shows the phase portrait diagram and the Poincare section of these responses showing that k = 0.05 produces a periodicity one response while k = 0.10 produces a periodicity two response.

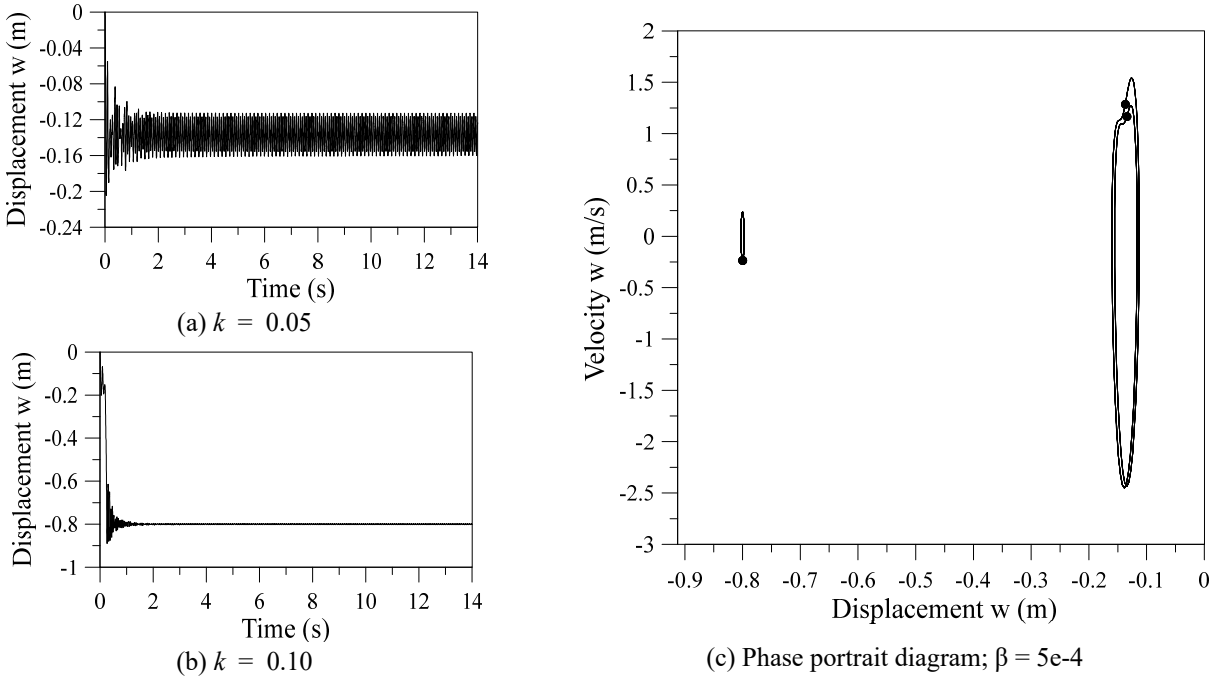

Figure 10 – H_h = 1.50 m; p_i = 79.5 kN/m²

CONCLUDING REMARKS

This work presents a nonlinear formulation and an analysis of a shallow parabolic conoidal shell using the finite element method with the software ABAQUS®. It is seen that increasing H_h changes the linear and nonlinear behavior of the shell by the presence of the imperfection function w_0 in the equilibrium system of equations. The results show that this geometry allows the occurrence of nonlinear phenomena, such as snap-back and snap-through. As the load increases the shell's natural frequency of vibration decrease up to the point where it become null, meaning the structure

became unstable. The nonlinear frequency-amplitude relation shows a softening behavior. For forced vibration, depending on the loading magnitude and the intensity of the dynamic perturbation, a dynamic jump occurs and the shell loses its stability through a saddle node bifurcation, this serves as a process to verify numerically the stability of the nonlinear equilibrium path of complex structures since the stable positions can be identified.

ACKNOWLEDGMENTS

This work was made possible by the financial support of the Coordination for the Improvement of Higher Level Personnel (CAPES) and the Brazilian Research Council (CNPq).

REFERENCES

CAVALCANTI, L. V. Análise da estabilidade e vibrações de cascas conoidais abatidas. Dissertação (Mestrado em Engenharia Civil) - Pontifícia Universidade Católica do Rio de Janeiro. Rio de Janeiro, p. 154. 2015.

CHAKRAVORTY, Dipankar; BANDYOPADHYAY, J. N.; SINHA, P. K. Finite element free vibration analysis of conoidal shells. Computers & structures, v. 56, n. 6, p. 975-978, 1995.

DEBONGNIE, Jean-François. Physical interpretation and generalization of Marguerre's shallow shell theory. International Journal of Engineering Science, v. 17, n. 4, p. 387-399, 1979.

GHOSH, Bimalednu; BANDYOPADHYAY, J. N. Bending analysis of conoidal shells using curved quadratic isoparametric element. Computers & structures, v. 33, n. 3, p. 717-728, 1989.

GHOSH, Bimalendu; BANDYOPADHYAY, J. N. Approximate bending analysis of conoidal shells using the Galerkin method. Computers & Structures, v. 36, n. 5, p. 801-805, 1990.

GONÇALVES, P. B.; SOARES, R. M. Buckling and nonlinear vibrations analysis of conoidal shells. In: 23rd ABCM International Congress of Mechanical Engineering, 2015, Rio de Janeiro, Brasil.

GONÇALVES, P. B.; SOARES, R. M. Buckling and Nonlinear Analysis of Conoidal Shells. In: ASME 2016 International Design Engineering Technical Conferences and Computers and Information in Engineering Conference. American Society of Mechanical Engineers, 2016. p. V008T10A017-V008T10A017.

HOTA, Sasank Sekhar; CHAKRAVORTY, Dipankar. Free vibration of stiffened conoidal shell roofs with cutouts. Journal of Vibration and Control, v. 13, n. 3, p. 221-240, 2007.

MORAIS, D. L. A. Análise estática não-linear de cascas conoidais. Dissertação (Mestrado em Engenharia Civil) – Universidade Federal de Goiás. Goiânia, p. 114. 2017.

NANDAKUMAR, K., CHATTERJEE, A., 2005. "Resonance, parameter estimation, and modal interactions in a strongly nonlinear Benchtop oscillator." *Nonlinear Dynamics*. Vol. 40, 149–167.

NAYAK, A. N.; BANDYOPADHYAY, J. N. Free vibration analysis and design aids of stiffened conoidal shells. Journal of engineering mechanics, v. 128, n. 4, p. 419-427, 2002.

RESPONSIBILITY NOTICE

The authors are the only responsible for the printed material included in this paper.